The Origin of Oscillations during Hydrogen Peroxide Reduction on GaAs Semiconductor Electrodes

ARTICLE *in* THE JOURNAL OF PHYSICAL CHEMISTRY · MARCH 1995

Impact Factor: 2.78 · DOI: 10.1021/j100011a041

2 AUTHORS:

Marc Koper
Leiden University
302 PUBLICATIONS **9,164** CITATIONS
SEE PROFILE

Daniel Vanmaekelbergh
Utrecht University
291 PUBLICATIONS **10,610** CITATIONS
SEE PROFILE

The Origin of Oscillations during Hydrogen Peroxide Reduction on GaAs Semiconductor Electrodes

Marc T. M. Koper*,† and Daniël Vanmaekelbergh‡

Departments of Electrochemistry and Condensed Matter, Debye Institute, Utrecht University, P.O. Box 80000, 3508 TA Utrecht, The Netherlands

Received: October 14, 1994; In Final Form: December 8, 1994®

The origin of current and potential oscillations during hydrogen peroxide reduction on n-type GaAs semiconductor electrodes is investigated. Impedance measurements clearly demonstrate that the current oscillations are caused by a negative impedance in conjunction with the electrolyte or external resistance. By considering a simple kinetic model which combines earlier mechanistic models proposed for the H_2O_2 and H^+ reduction on GaAs, it is shown that oscillations can occur only if the negative impedance is caused by an anomalous dependence of the band bending on the electrode potential, i.e., if an increase of the Fermi level of the n-type semiconductor results in an increase in the band bending. This effect is assumed to be caused by a hydride layer formed electrochemically during the concomitant proton reduction. Impedance measurements confirm the role of the band-bending anomaly.

Introduction

The electrochemical reduction of hydrogen peroxide is a widely studied reaction because of the application of H_2O_2 as an etchant in semiconductor device fabrication and because it is a side reaction in oxygen reduction. A number of authors have reported the occurrence of spontaneous current or potential oscillations in this reaction, on a variety of electrode materials.[1-9] Although several details of the reduction mechanism of H_2O_2 on various electrodes are known,[10-13] no attempt has as yet been made to explain the oscillatory behavior beyond the phenomenological level.

In a previous paper in this journal,[8] we described the occurrence of (complex) current and potential oscillations on n- and p-type GaAs semiconductor electrodes. Since the kinetics of this reaction has been studied in some detail by Minks *et al.*,[12,13] the H_2O_2 reduction on GaAs could serve as an interesting starting point for studying oscillations at semiconductor electrodes. Although oscillations at semiconductor electrodes are usually bracketed with oscillations at metal electrodes, there are some interesting new phenomena that deserve special attention, such as photocurrent oscillations and oscillatory light emission. Moreover, as the potential distribution across the semiconductor/electrolyte interface is markedly different from that across the metal/electrolyte interface, it is interesting to study how this affects the possibility of instabilities and oscillations.

The present paper is devoted to an elucidation of the origin of the current oscillations at the n-type material. First, it will be shown experimentally that the negative polarization slope observed in the H_2O_2 reduction on n-type GaAs becomes destabilized due to the presence of an external ohmic drop, giving rise to the sustained current oscillations. This is, of course, a well-known fact from the theory of electrochemical oscillations,[14] which can also be seen from the potentiostatic impedance measurements. Next, it will be shown how the model suggested by Minks *et al.*[13] can be modified to incorporate an explanation of the oscillations. The main point here is that a stability analysis of this modified model will allow us to show that not just any explanation of the observed negative polarization slope will result in oscillations. Only an explanation invoking an anomalous dependence of the semiconductor band bending on the interfacial potential can explain oscillations, and the results of the impedance measurements will confirm this "band-bending anomaly" experimentally. Finally, we discuss what the modified Minks model cannot (yet) explain (basically this involves its inability to explain the galvanostatic potential oscillations) and how this feature is related to the impedance data.

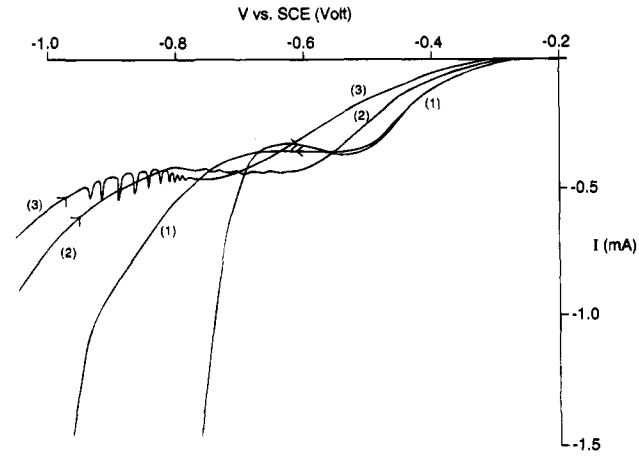

Figure 1. Cathodic current–potential scan for an n-type GaAs electrode in 0.1 M H_2O_2 and 1 M H_2SO_4 at 40 °C. Scan rate 2 mV/s. (1) $R_s = 0\ \Omega$; (2) $R_s = 200\ \Omega$; (3) $R_s = 400\ \Omega$.

Experimental Section

The experiments were carried out in a thermostatically controlled electrochemical cell in a three-electrode configuration. The working electrode consisted of a GaAs single-crystal wafer (3.85 mm in diameter) glued onto a copper substrate and embedded in a PVC holder, which was screwed onto a rotating disk unit. The n-type ⟨100⟩ material, having a doping level of $\sim 10^{18}$ cm^{-3} (Si), was purchased from MCP Electronic Materials Ltd. The counter electrode was a large platinum sheet, and the reference electrode was a saturated calomel electrode (SCE). All potentials are given with respect to the SCE.

† Department of Electrochemistry.
‡ Department of Condensed Matter.
® Abstract published in *Advance ACS Abstracts*, February 15, 1995.

0022-3654/95/2099-3687$09.00/0

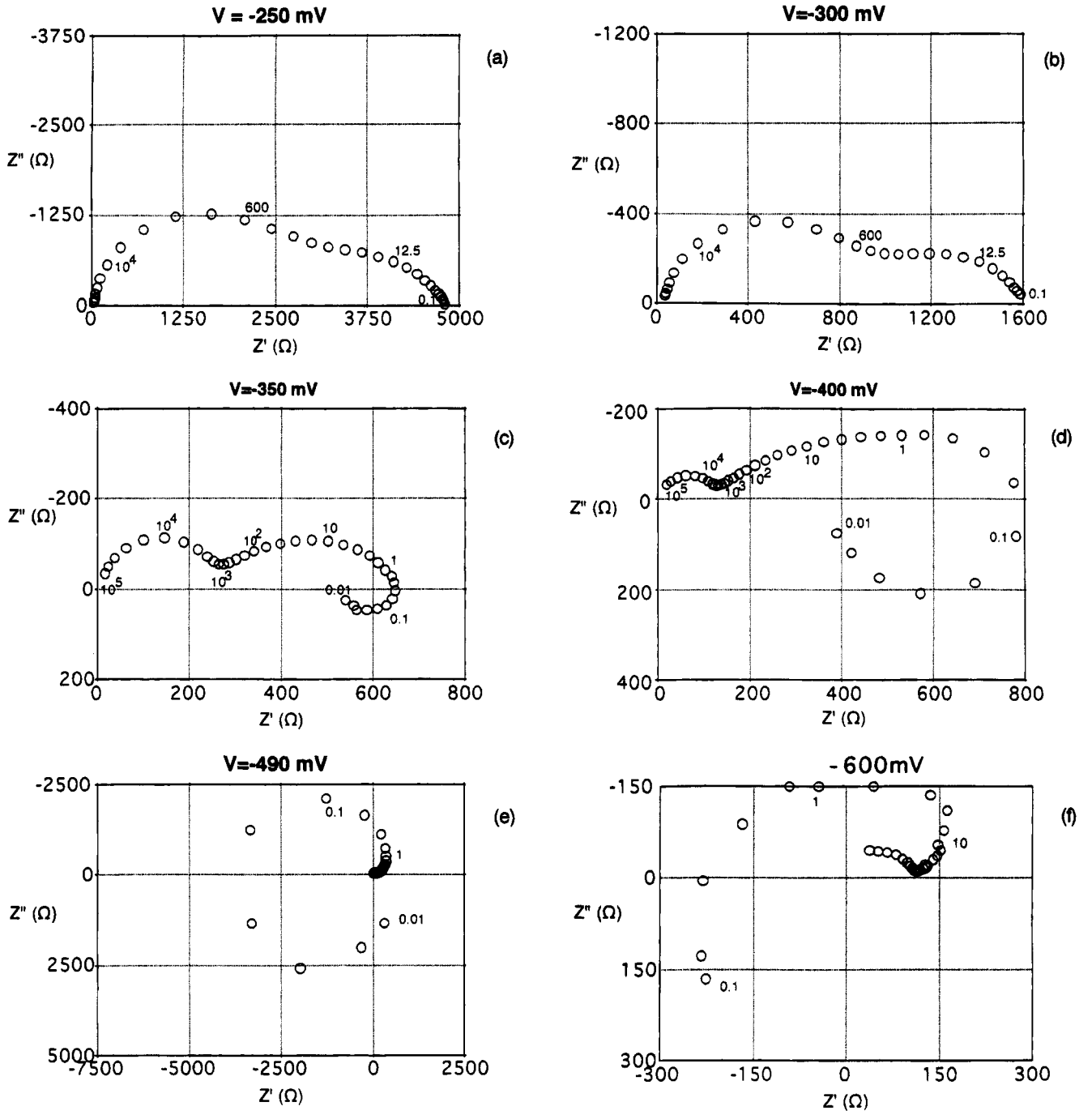

Figure 2. Impedance plots of the complex cell impedance $Z' + iZ''$, $i = -1^{1/2}$, determined at the indicated potential values. Indicated frequencies in Hz.

Potential control was performed by a Wenking ST72 potentiostat, connected to a Wenking VSG83 voltage scan generator. For impedance measurements, a Solartron 1250 frequency analyzer was used in combination with a PAR 273A potentiostat. The perturbation amplitude was 10 mV, and the perturbation frequency ranged from 2×10^5 to 0.01 Hz.

The experiments were carried out with a solution of 0.1 M H_2O_2 (Merck, 30% perhydrol) in 1.0 M H_2SO_4 (Merck). During the experiments, the electrode rotation rate was 1000 rpm and the cell temperature was maintained at 40 °C.

Results

Figure 1 shows three current−voltage scans (1) taken in the absence of an external resistance, (2) taken with an external resistance of 200 Ω, exhibiting small current oscillations in the region of negative polarization slope, and (3) taken with an external resistance of 400 Ω, exhibiting more pronounced current oscillations. The "critical" resistance value of ca. 200 Ω is indeed about a factor of 10 larger than the electrolyte resistance itself of ~15 Ω, a value that is sufficient to induce current oscillations for a 10-fold higher concentration of H_2O_2 as was used in our previous publication.[8] This figure is a clear confirmation of the fact that the negative slope is destabilized in the presence of a sufficiently large external potential drop. The hysteresis observed in the scans is due to the non-zero scan rate.[8]

Impedance measurements were carried out at various potentials on polarization curve 1 in Figure 1, in the absence of an external ohmic resistor. Figure 2 illustrates a typical sequence of plots.

At potentials positive with respect to −0.2 V (in the (semi)-polarizable potential region), the impedance plot (Im vs Re) is a semicircle, the resistance of which is (very) large and the capacitance of which obeys the Mott−Schottky relationship. From measurements between −0.2 and 1.0 V at 10^4 Hz, a flatband potential of −0.9 V and a donor concentration (N_D) of 1.4×10^{18} cm^{-3} are obtained (in fair agreement with the specifications of the supplier). At potentials negative of −0.2 V, a net cathodic current flows and the impedance develops from one to two partly overlapping semicircles (V = −250, −300 mV, Figure 2a and b). At −350 and −400 mV, an inductive loop appears in the impedance plot at very low frequencies (Figure 2c and d). At potentials more negative than −450 mV, there is a transition to a negative real part at low frequencies, as illustrated in the plots taken at −490 and −600 mV (Figure 2e and f). It should be remarked, however, that the data in Figure 2e and f at the two or three lowest frequencies do not acquire the desired accuracy within 10 sine waves (in contrast to the results in Figure 2c and d), which makes their reliability questionable.

The impedance data are consistent with the stability features of the system under the various types of electric control.[15,16] In the presence of the external ohmic resistor, the plot of Figure 2e would exhibit a so-called Hopf bifurcation for an external resistance value of ca. 3500 Ω, that of Figure 2f for 250 Ω, the latter value being in agreement with the onset of oscillations in the scans of Figure 1. As is well-known,[17] a Hopf bifurcation (i.e., a critical situation in which the linearized system produces an undamped sine wave) is, in practice, an excellent (though strictly speaking not sufficient) indication of sustained nonlinear oscillations. Also, the impedance plot of Figure 2e is the type of plot expected to lead to potential oscillations under galvanostatic conditions.[15,16] These are indeed easily observable, on both n- and p-type electrodes.[8,16]

Model

Kinetics of the H_2O_2 Reduction at GaAs Semiconductor Electrodes. It is well established that the reduction of H_2O_2 at metal and semiconductor electrodes occurs via two consecutive electron-transfer reactions, with the OH• radical as an (unstable) intermediate.[10,11] From the observation that, at p-type electrodes, H_2O_2 is reduced only under illumination, Memming[11] (who studied the system at GaP) concluded that at least one step of the mechanism involves a (photoexcited) conduction band electron:

$$H_2O_2 + e_{CB}^- \rightarrow HO^\bullet + OH^-$$

$$HO^\bullet \rightarrow OH^- + h_{VB}^+$$

where the first step is rate determining and in the second step the unstable OH• radical is reduced by injecting a hole into the valence band. This mechanism also explains the experimentally observed "current doubling" at p-type materials, since for every photon absorbed two electrons are transferred across the semiconductor/electrolyte interface.

There is much experimental evidence to show that GaAs is etched chemically by H_2O_2 according to the overall reaction

$$3H_2O_2 + GaAs \xrightarrow{k_{ch}} 3H_2O + Ga^{3+} + AsO_3^{3-}$$

Experiments by Minks *et al*[12] have shown that rates of the reduction and etching to be correlated, and Memming's mechanism was revised[13] to the extent that both processes were assumed to proceed via a common precursor, postulated to be some chemisorbed H_2O_2 intermediate. This model was shown to account qualitatively for most of the experimental results at n- and p-type GaAs in H_2O_2 solutions of moderate concentration and temperature. The main features can be summarized in the following reaction scheme:

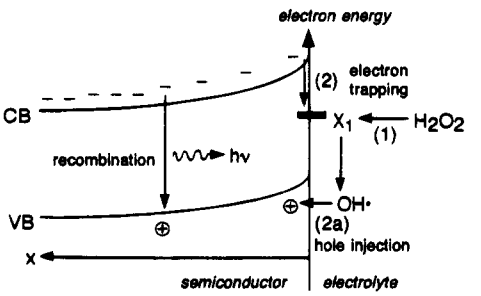

Figure 3. Energy level representation of the H_2O_2 reduction according to the model of Minks *et al.*[13]

$$H_2O_2 + X_0 \xrightarrow{k_1} X_1^{+\ OH^-_{OH^\bullet}} \quad (1)$$

$$X_1^{+\ OH^-_{OH^\bullet}} + e_{CB}^- \xrightarrow{k_2} X_0OH^\bullet + OH^- \quad (2)$$

$$X_0OH^\bullet \xrightarrow{fast} X_0 + OH^- + h_{VB}^+ \quad (2a)$$

In the first step (rate constant k_1), H_2O_2 is chemisorbed onto a free surface site X_0, creating a surface intermediate consisting of an electron-deficient surface bond X_1^+, an OH^- ion, and an OH• radical (the notation employed is naive). This surface intermediate (where the electron-deficient surface bond has an energy level in the band gap) is assumed to be the precursor for further reduction and chemical etching. Further reduction takes place via reaction 2, in which X_1^+ acts as an effective trap for a conduction band electron, leading to a restored surface bond and OH^- in the solution. The sequence of processes 1 and 2 is similar to recombination of a hole, trapped in a surface bond, with a conduction band electron. In a subsequent step, (2a), the unstable OH• rapidly injects into the valence band a hole, which, in an n-type semiconductor, recombines with a conduction band electron at the surface or in the bulk. Recombination in the bulk can be radiative, giving rise to electroluminescence. (See Figure 3.)

At low overpotential, the electron capture (reaction 2) limits the cathodic current, due to the limited availability of conduction band electrons at the interface. At higher overpotential (i.e., smaller band bending), Minks *et al.*[12] observed a potential-independent current, which they attributed to the potential-independent chemisorption reaction (1). However, at higher temperature (40 °C), in the reverse scan (that is, in the anodic direction), the current−voltage curve displays a region of negative slope, as can be seen in Figure 1. A similar passivation effect has been observed during H_2O_2 reduction at Ge,[18] $CuFeS_4$,[2,4] $CuInSe_2$,[6] Pt,[9] and Ag.[3] Gerischer and Mindt[18] suggested that the negative slope at Ge is due to a competing reaction of H^+ with the Ge radical surface sites at which they assumed the H_2O_2 reduction to proceed; at Pt, the passivaiton region was shown to be shifted cathodically with increasing solution pH.[9] For GaAs, it seems reasonable to assume a similar involvement of the H^+ reduction with the negative slope. According to Gerischer *et al.*,[19] the hydrogen evolution at GaAs involves two consecutive conduction band processes:

$$X_0 + H^+ + e_{CB}^- \underset{k_{-3}}{\overset{k_3}{\rightleftharpoons}} X_0H^\bullet \quad (3)$$

$$X_0H^{\bullet} + H^+ + e_{CB}^- \xrightarrow{k_4} X_0 + H_2 \quad (4)$$

In this scheme, it is conceivable that the negative slope is caused either by a competition for X_0 adsorption sites between reactions 1 and 3 or by a (dramatic) shift in the energy of the band edges at the surface induced by the H-surface intermediate (this will be worked out in more detail below).

So far, we have not paid any attention to the exact nature of the X_0 adsorption site. In a simplistic view, this would simply be a bare GaAs surface entity, but since it is well-known that acid–base equilibria establish at the GaAs surface,[20] a GaAs site with the proton attached to it is probably more realistic (for the solutions of low pH, as used above). Although the view of X_0 as a site with the H^+ already attached to it invalidates the idea of a competitive adsorption between H_2O_2 and H^+, we will leave the possibility of competitive adsorption in tact in the kinetic equations below, as the analysis will allow us to show that although one can employ the idea of competitive adsorption to explain the negative slope, it will not explain the oscillations.

Reactions 1–4 result in the following rate equations for the time evolution of the fractional coverages of the surface intermediates X_1 and $X_0H^{\bullet}$:

$$d\theta_1/dt = v_1 - v_2$$

$$d\theta_H/dt = v_3 - v_4 \quad (5)$$

with

$$v_1 = k_1 (1 - \theta_1 - \theta_H) - k_{ch}\, \theta_1$$

$$v_2 = k_2 n_s(\phi_{sc})\theta_1$$

$$v_3 = k_3(\phi_H) n_s(\phi_{sc})(1 - \theta_1 - \theta_H) - k_{-3}(\phi_H)\theta_H$$

$$v_4 = k_4(\phi_H) n_s(\phi_{sc})\theta_H$$

where n_s is the concentration of conduction band electrons at the surface (in cm^{-3}), k_1, k_{ch}, and k_{-3} have dimension s^{-1}, and k_3, k_2, and k_4 have dimension $cm^3\ s^{-1}$ (note that the chemical etch rate is assumed to be first-order in θ_1 and has been incorporated into v_1 for convenience). Following the suggestion by Minks *et al.*[12,13] that the rate-determining step in reaction 1 is the adsorption of the H_2O_2 onto a free surface site and the subsequent electron tunneling from the surface bond to the hydrogen peroxide is relatively fast, the rate constant of reaction 1 is assumed to be potential independent. The other rates follow Tafel-like relationships:

$$n_s = N_D \exp(-f\phi_{sc}), \quad k_3 = k_3^0 \exp(-\alpha_3 f\phi_H), \quad k_{-3} = k_{-3}^0 \exp((1 - \alpha_3) f\phi_H), \quad k_4 = k_4^0 \exp(-\alpha_4 f\phi_H) \quad (6)$$

where N_D stands for the donor concentration of the n-type semiconductor, α stands for transfer coefficients, and $f = e/kT$ (with e being the elementary charge, k Boltzmann's constant, and T temperature).

Charge Balance. In addition to the mass balances (eq 5), a charge balance equation is needed for a reduction process at an n-type semiconductor (see Figure 4). In general, transfer of charge carriers across the semiconductor/electrolyte by an electrochemical reaction can result in a measurable current in two different ways:[21]

(i) If the majority carrier tunnels directly through the Helmholtz layer (as in reaction 3), this leads to an instantaneously measurable current (assuming there is instantaneous equilibration of majority carriers in the depletion layer), represented by a single current pathway connected in parallel with the Helmholtz and the depletion layers. This current will be referred to as j_{maj}.

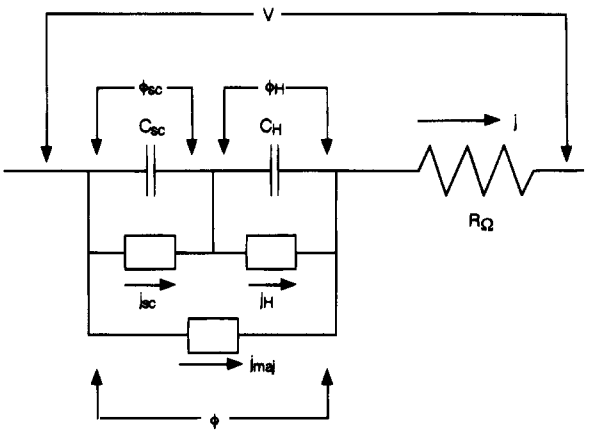

Figure 4. Equivalent circuit representation of the charge balance at the semiconductor/electrolyte interface.

(ii) If, however, the transfer of an electronic charge across the entire interfacial region occurs in two steps, via a localized surface intermediate (for instance, the precursor formed in reaction 1), a current in the external circuit is measured after recombination of the intermediate with a majority carrier followed by instantaneous equilibration. Hence, in a time-resolved view, there are two consecutive steps connected with the currents j_H and j_{sc}, respectively (see Figure 4). The difference between these two currents is used to charge the two capacitors, and if a stable steady state exists, this continues until the potential differences across them, ϕ_H and ϕ_{sc}, are such that j_H and j_{sc} become equal. In what follows, ϕ_{sc} is the potential in the bulk of the semiconductor minus the potential at the surface, and ϕ_H is the potential at the surface minus the potential just outside the Helmholtz double layer. Taking into account the ohmic electrolyte resistance, R_Ω, the total equivalent cell circuit takes the form of Figure 4.

It is possible to derive a single differential equation for the total interfacial potential (ϕ) by a straightforward application of Kirchhoff's laws. First it is recognized that

$$C_{sc}\frac{d\phi_{sc}}{dt} + j_{sc} = C_H\frac{d\phi_H}{dt} + j_H \quad (7)$$

It is also clear that

$$C_H\frac{d\phi_H}{dt} + j_H + j_{maj} = \frac{V - \phi}{AR_\Omega} = j \quad (8)$$

V is the applied potential with respect to some reference electrode, A the electrode surface area, and j the total current density. Using $\phi = \phi_H + \phi_{sc}$ and relation 7, $d\phi_H/dt$ can be written in terms of $d\phi/dt$, from which the desired differential equation follows:

$$C_{sc}\beta\frac{d\phi}{dt} = \frac{V - \phi}{AR_\Omega} - \beta j_{sc} - (1 - \beta) j_H - j_{maj} \quad (9)$$

where

$$\beta = \frac{C_H}{C_{sc} + C_H}$$

(Throughout it is assumed that the potential dependence of C_{sc}

and C_H can be neglected.) The role of surface intermediates can be taken into account by realizing that the total charge density on the semiconductor should equal that in the Helmholtz layer:

$$q_{sc} + q_{ss} = -q_H \text{ or } dq_{sc} + dq_{ss} = -dq_H \quad (10)$$

where q_{sc} is the total charge density corresponding to uncompensated donors in the depletion layer and q_{ss} denotes the charge stored in surface states. Similarly, one has

$$\phi = \phi_{sc} + \phi_H \text{ or } d\phi = d\phi_{sc} + d\phi_H \quad (11)$$

and since $dq_{sc} = C_{sc}\, d\phi_{sc}$ and $dq_H = -C_H\, d\phi_H$, it follows that

$$d\phi_{sc} = \beta\, d\phi - \sum_i \gamma_i\, d\theta_i \quad (12)$$

$$d\phi_H = (1-\beta)d\phi + \sum_i \gamma_i\, d\theta_i \quad (13)$$

where we have taken

$$dq_{ss} = \sum_i \xi_i e \Gamma_m\, d\theta_i$$

(assuming—for simplicity—that all surface states and adsorbates compete for the same sites, with Γ_m being the total number of sites per unit area and θ_i the fractional coverage of species i) so that the parameter γ_i, defined as $-(\partial\phi_{sc}/\partial\theta_i)_{\phi,\theta_{j\neq i}}$, is given by

$$\gamma_i = \frac{\xi_i e \Gamma_m}{C_{sc} + C_H} \quad (14)$$

This parameter measures the change induced in the band bending by surface state i. If an integral number of elementary charges are involved in the creation or adsorption of the surface intermediate, ξ_i equals the normal valency z_i. In general, however, ξ_i can be a noninteger due to geometrical effects, a change in the dipole environment of the surface state, partial charge transfer, etc.[22] The parameter ξ_i is also known as the electrosorption valency.[22] A typical order of magnitude of γ, with $\xi = 1$, $\Gamma_m = 10^{13}$–10^{14} cm^{-2}, and $C_H = 10$ μF cm^{-2}, is 0.16–1.6 V.

Equations 10 and 11 can be integrated to give

$$\phi_{sc} = \beta\phi - \sum_i \gamma_i\theta_i + \text{cst} \quad (15)$$

$$\phi_H = (1-\beta)\phi + \sum_i \gamma_i\theta_i - \text{cst} \quad (16)$$

where the integration constant (cst) is the flatband potential in the absence of surface states.

Linear Stability Analysis. The considerations of the two previous subsections can now be combined and subjected to a linear stability analysis to investigate the possibility of a Hopf bifurcation. To simplify matters, we make the following assumptions:

(i) It will be assumed that $C_{sc} \ll C_H$ so that $\beta = 1$ and the total (cathodic) faradaic current density can be equated to

$$j_{F,tot} = -e\Gamma_m(2\nu_2 + \nu_3 + \nu_4) \quad (17)$$

where the factor 2 stems from the fast hole injection (process 2a) (and subsequent recombination) immediately following reaction 2. This assumption is clearly very reasonable.

(ii) The hydrogen production reaction (4) will be neglected because in the potential region of the current oscillations there is no appreciable current due to the hydrogen evolution.[8] (However, very recently, Pohlmann *et al.*[23] have shown experimentally that there is a periodic hydrogen evolution accompanying the galvanostatic potential oscillations during H_2O_2 reduction on $CuInSe_2$, but its reduction current is small with respect to the H_2O_2 reduction current.)

(iii) Because an analytical stability analysis is considerably easier if it is restricted to two variables, it will be assumed that reaction 3 is reversible and in a quasi-stationary state so that the hydrogen-intermediate coverage parametrically depends on ϕ and θ_1:

$$\theta_H(\phi,\theta_1) = \frac{1-\theta_1}{1 + \dfrac{k_{-3}}{k_3 n_s}} \quad (18)$$

In the Discussion section, evidence will be presented that removal of this assumption does not have consequences for the most important conclusion of the stability analysis.

(iv) The (nonstationary) current associated with reaction 3 will also be neglected, since it involves at most a monolayer (no $d\theta_H/dt$ term in the charge balance).

(v) The influence of θ_1 on the potential distribution will be neglected; i.e., $\gamma_1\theta_1 \approx 0$ (this assumption is supported by the experimental observation that the flatband potential is hardly dependent on the H_2O_2 bulk concentration[24]), which holds whenever $k_1 \ll k_2 n_s + k_{ch}$. However, a change in θ_H will be assumed to modify substantially the potential distribution, following eqs 15 and 16 with $\beta = 1$ so that

$$\phi_{sc} = \phi - \gamma_H\theta_H + \text{cst}, \quad \phi_H = \gamma_H\theta_H - \text{cst} \quad (19)$$

The stability analysis can now be carried out in two apparently different but fully equivalent ways. One way is to write the differential equations for ϕ and θ_1, linearize them about the stationary state, evaluate the eigenvalues of the linearized Jacobian matrix, and check for the possibility of a pair of complex conjugate eigenvalues with vanishing real part, i.e., a Hopf bifurcation.[17] The other way calculates the impedance response of the system under potentiostatic control, perhaps even reduces it to an equivalent circuit, and then evaluates the stability of the circuit in the presence of an external resistor or under constant current load, by employing the Nyquist stability criterion of electrical control engineering.[15,16] Although the second way may be more familiar to electrochemists, the first way is more direct and will therefore be used here. However, in the Discussion section, we will indicate what the consequences of the analysis are in terms of the impedance behavior of the model.

Assumptions i–v reduce the model to two coupled differential equations:

$$C_{sc}\frac{d\phi}{dt} = \frac{V-\phi}{AR_\Omega} + e\Gamma_m\nu_2, \quad \frac{d\theta_1}{dt} = \nu_1 - \nu_2 \quad (20)$$

with

$$\nu_1 = k_1(1-\theta_1-\theta_H(\phi,\theta_1)) - k_{ch}\theta_1, \quad \nu_2 = k_2 n_s(\phi_{sc})\theta_1$$

It is convenient to rewrite this as

$$\epsilon\frac{d\phi}{dt} = \frac{V-\phi}{R} + \nu_2 \equiv F(\phi,\theta_1)$$

$$\frac{d\theta_1}{dt} = v_1 - v_2 \equiv G(\phi,\theta_1) \tag{21}$$

where the potentials have been scaled by a factor f, $R = AR_\Omega e\Gamma_m$, and $\epsilon = C_{sc}/fe\Gamma_m$ ($f = e/kT \approx 39$ V^{-1}). As $e\Gamma_m \approx 1.6-16\ \mu$C cm^{-2} (if $\Gamma_m = 10^{13}-10^{14}$ cm^{-2}), it follows that the dimensionless parameter ϵ is likely to satisfy $0 < \epsilon \ll 1$. This implies that the interfacial potential relaxes on a much faster time scale than θ_1. This inequality will be useful further on.

The linear stability analysis leads to a number of awkward expressions and has therefore been relegated to the Appendix so as not to distract from the main argument. The conclusions can be summarized as follows.

Under conditions of a fixed applied potential V, the two prime conditions for having a Hopf bifurcation are as follows:

(i) $\partial v_2/\partial\phi > 0$, which means $d\phi_{sc}/d\phi < 0$; i.e., there should be a potential region where the electron trapping (reaction 2) becomes less effective with increasing overpotential, caused by an anomalous band-bending effect, as the band bending has to increase with an increase of the Fermi energy level (i.e., decreasing ϕ).

(ii) $1/R$ should be sufficiently small; i.e., the external or cell resistance has to be sufficiently large.

The condition for a Hopf bifurcation becomes particularly simple for the specific but realistic case that $\epsilon \ll 1$; i.e., the typical relaxation time for the potential is (much) smaller than for the concentration of the surface intermediate X_1:

$$\frac{\partial v_2}{\partial\phi} = \frac{1}{R}(>0), \qquad \frac{\partial v_1}{\partial\phi} < \frac{1}{R} \tag{22}$$

where the latter condition is normally satisfied (see the Appendix).

Under conditions of a fixed applied current J (galvanostatic control), the condition for a Hopf bifurcation cannot be satisfied within the assumptions of the above model.

Most of these conclusions are similar to results recently derived from a stability analysis of a simple model of an electrocatalytic surface reaction.[25] We find also that a negative slope caused by a competitive adsorption between an adsorbing electroactive species and a "poisoning" species cannot account for oscillations and that a "simple" negative slope does not give rise to galvanostatic potential oscillations. What is new—although "in retrospect" also not very surprising—is that we find that for the H_2O_2/GaAs interface, the oscillations must be related to an anomalous dependence of the band bending on the interfacial potential ϕ and that the relaxation of the Helmholtz double-layer potential does not play any role (this is, of course, a consequence of our assumption $C_{sc} \ll C_H$). Below, it will be shown that this peculiar band-bending anomaly can indeed be confirmed experimentally.

Finally, it should be checked whether our simple model can actually satisfy the primary instability condition $d\phi_{sc}/d\phi < 0$. From eq 19, it follows that

$$\frac{d\phi_{sc}}{d\phi} = 1 - \gamma_H \frac{d\theta_H}{d\phi} \tag{23}$$

Since this is a condition to be evaluated in the steady state, eq 18 can be used and, if $k_1 \ll k_2 n_s + k_{ch}$, be simplified to

$$\theta_H = \frac{1}{1 + \dfrac{k_{-3}}{k_3 n_s}} \tag{24}$$

Inserting eq 19 into eq 24, the denominator no longer depends on θ_H and the derivative is easily taken, yielding (after some manipulation)

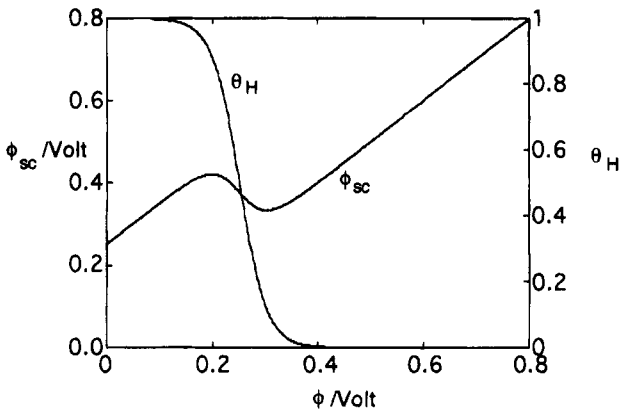

Figure 5. Band bending ϕ_{sc} and hydride coverage θ_H as a function of the electrode potential ϕ as predicted by eqs 13 and 23. $\beta = 1$, cst = -1 V (=flatband potential), $\gamma_H = -0.25$ V, $k_{-3}^0/k_3^0 = 10^{-10}$ cm^{-3}, $N_D = 10^{18}$ cm^{-3}.

$$\frac{d\phi_{sc}}{d\phi} = 1 + \frac{e\gamma_H}{kT}\theta_H(1 - \theta_H) \tag{25}$$

This shows that γ_H should be negative and in absolute value larger than $[kT/e][\theta_H(1 - \theta_H)]^{-1}$, giving values of ca. 0.1, 0.28, and 2.5 V for $\theta_H = 0.5$, 0.1, and 0.01, respectively, in principle perfectly reasonable values. The negative sign of γ_H corresponds to a decrease of positive surface charge and hence to an increase in energy of the band edges at the surface by increasing θ_H, as such rendering slower the further reduction of the H_2O_2. This peculiar band-bending dependence on the electrode potential is illustrated in Figure 5 for $\gamma_H = -0.25$ V and a rather arbitrary value of $k_{-3}^0/k_3^0 = 10^{-10}$.

It is important to emphasize that if the "filling" of the X_0/X_0H^+ surface states by reaction 3 is assumed to be independent of the Helmholtz layer potential, i.e., if k_3 and k_{-3} are taken independent of ϕ_H, the condition $d\phi_{sc}/d\phi < 0$ cannot be satisfied, but instead, the more familiar inequality $0 < d\phi_{sc}/d\phi < 1$ is satisfied for a negative value of γ_H (a positive value of γ_H would correspond to a surface state which decreases the band bending; for this there is no experimental evidence, as will be shown in the next section). Apparently, a "classical" nonelectrochemical filling of surface states will not lead to the instability requirement $d\phi_{sc}/d\phi < 0$.

Finally, it is stressed that the condition for an oscillatory instability $d\phi_{sc}/d\phi < 0$ applies uniquely to electrochemical reactions which take place via an adsorbed intermediate and occur under depletion layer control; i.e., $C_{sc} \ll C_H$. For the present system, the analysis given above suggests that the instability is related to a poisoning species (that we assume to be a kind of hydride surface layer) that acts on the energy factor (through the band bending) of the charge-transfer step in the H_2O_2 reduction.

Experimental Confirmation of the Band-Bending Anomaly. It will now be shown that the existence of a potential region where $d\phi_{sc}/d\phi < 0$ can indeed be confirmed experimentally.

A prominent feature in all the impedance plots of Figure 2 is the persistence of a distinct semicircle at the highest frequencies (in the plot of Figure 2e, it is less clear). We can take the high-frequency loop at $V = -400$ mV as an example. The maximum of this loop lies at ca. $2\pi \times 2.6 \times 10^4$ rad s^{-1}, and its diameter is approximately 120 Ω, from which a capacity of ~0.4 μF cm^{-2} is calculated. This clearly corresponds to the semiconductor depletion layer. The resistance of the loop should correspond

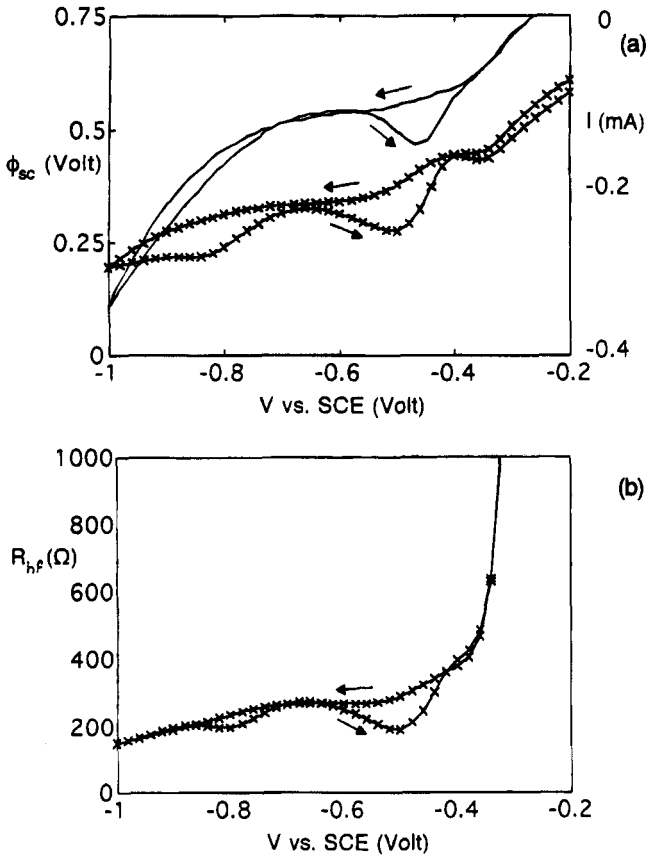

Figure 6. (a) Band bending ϕ_{sc} (line with crosses) as extrapolated from eq 26 from a measurement at 50 kHz and the corresponding reduction current (solid line) as a function of the applied potential V. (b) High-frequency resistance parallel to C_{sc} at 50 kHz as a function of V. The GaAs sample used for this experiment had a lower doping level than that used in Figure 1.

to a situation for which all surface intermediates are frozen in their stationary state and is therefore expected to be directly proportional to $-\partial n_s/\partial\phi = en_s/kT$.

From this small loop, the semiconductor depletion layer capacity and the high-frequency resistance R_{hf} can be determined at any desired potential and, therefore, the band bending as a function of the applied potential. Results of such a measurement (at 50 kHz) are presented in Figure 6. (These measurements were carried out at six different (high) frequencies, and the data were fitted to a circuit consisting of a parallel connection of a condensor and a resistor; although there was some frequency dispersion, the qualitative picture was the same at all frequencies). The band bending ϕ_{sc} as determined from the Mott-Schottky equation[26]

$$C_{sc}^{-2} = \left(\frac{2}{e\epsilon\epsilon_0 N_D}\right)\left(\phi_{sc} - \frac{kT}{e}\right) \tag{26}$$

and the high-frequency resistance are plotted in parts a and b of Figure 6, respectively. The hysteresis in both figures is due to the non-zero scan rate.

In Figure 6a, it is seen that between −200 and −350 mV changes in the applied potential are accommodated entirely across the depletion layer (slope $d\phi_{sc}/d\phi = 1$, $V \approx \phi$ as the ohmic potential drop is small). Around −350 mV, the first deviation from this "ideal behavior" occurs, which we find difficult to interpret. In the reverse scan, there is a more dramatic deviation from ~ −650 to ~ −450 mV where a more negative applied potential (and thus a rise in the Fermi level) causes an increase in the band bending. This region corresponds to the region of negative slope in the reverse $I-V$ scan (as illustrated) and shows that the negative slope is related to an anomalous dependence of the band bending on the interfacial potential; i.e., $d\phi_{sc}/d\phi < 0$. This result is consistent with our theoretically derived condition for the possibility of current oscillations at the H_2O_2/GaAs interface. The anomaly is also apparent from the plot of R_{hf} vs V; the increase in resistance in the potential region from −0.5 to −0.65 V is due to a decrease in the number of available conduction band electrons at the surface owing to the increased band bending.

As outlined in the previous section, the model explains the region of negative $d\phi_{sc}/d\phi$ by the formation of a hydride surface layer. In impedance measurements in a solution without H_2O_2, there is indeed a deviation from ideal behavior in the potential region from −650 to −450 mV (whereas in the other potential regions $d\phi_{sc}/d\phi \approx 1$), but the slope does not become negative. Measurements in which the depletion layer capacity was measured at 0.0 V after electrode pretreatment at potentials between −300 and −700 mV for 30 s also indicate that as the pretreatment potential is made more negative, a surface intermediate is formed which increases the band bending, though not to an extent as dramatic as for solutions containing H_2O_2. It is clearly desirable to resolve this important point, though it is doubtful whether this can be achieved by impedance measurements alone. In this respect, it is interesting to note that a similar effect has been observed in the H_2O_2 reduction at $CuInSe_2$ by Cattarin *et al.*[6] with a different technique. These authors measured the potential dependence of the electroreflectance of the interface, a signal which is a measure of the concentration of free electrons at the surface. In the potential region where a negative slope occurred in the polarization curve and current oscillations usually take place, a marked increase in electroreflectance with increasingly negative potential is observed. This can be interpreted as evidence for a band-bending anomaly.

Discussion

In this section, it will be discussed how the stability analysis of the Model section relates to the impedance behavior of the model and how the latter relates to the experimental impedance plots. The impedance analysis will also provide us with an argument that a finite rate of formation of the hydride layer, i.e., removal of quasi-stationarity assumption iii in the Model section, will leave in tact the possibility of a Hopf bifurcation. Finally, we will discuss the relation of our model to a model recently proposed by Pohlmann *et al.*[23] for the oscillatory H_2O_2 reduction on $CuInSe_2$.

Following the analysis of ref 27, an expression can be derived for the faradaic (or recombination[21]) impedance of a reaction with a adsorbed intermediate, which follows the rate equation:

$$\frac{d\theta_1}{dt} = k_1(1 - \theta_1 - \theta_H(\phi)) - k_{ch}\theta_1 - k_2\theta_1 n_s(\phi_{sc}) \tag{27}$$

where the dependence of θ_H on θ_1 has been neglected. Disregarding contributions of changes of θ_H to the faradaic current, the equivalent cell circuit of Figure 7 is obtained, with

$$R_\infty = \left[\frac{e|j|}{kT}\frac{d\phi_{sc}}{d\phi}\right]^{-1} \qquad |j| = 2e\Gamma_m k_2 n_s \theta_1$$

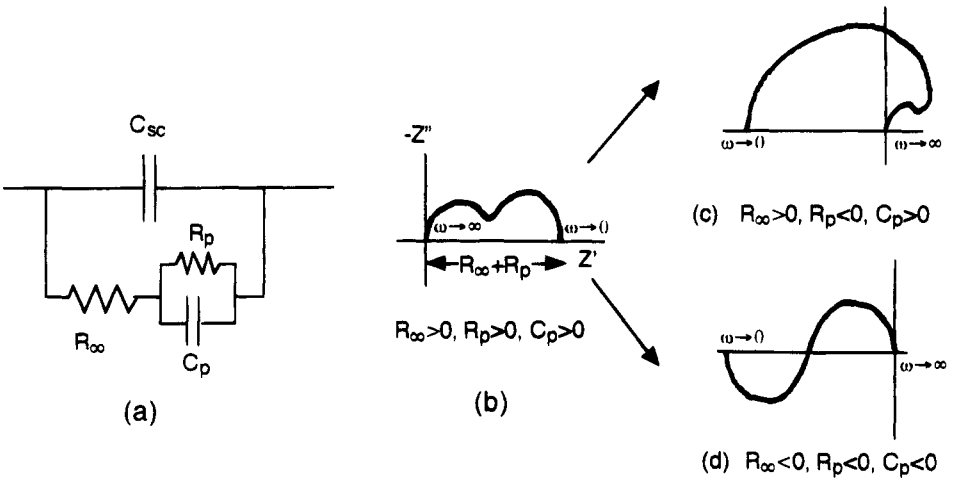

Figure 7. (a) Equivalent cell circuit for the model with rate equation 27; symbols are defined in the text. (b) Complex impedance plot for the circuit in the case positive R_∞, R_p, and C_p. (c and d) Two alternatives for a transition from a complex impedance plane plot with positive polarization slope $R_\infty + R_p > 0$ to negative polarization slope $R_\infty + R_p < 0$ with $R_p < 0$ and $R_\infty > 0$ (c) or with R_∞ and $R_p < 0$ (d).

$$C_p = \frac{1}{k_2 n_s R_\infty}\frac{R_H}{R_H + R_\infty} \qquad R_p = \frac{R_\infty(1 + R_\infty/R_H)}{\frac{k_1 + k_{ch}}{k_2 n_s} - R_\infty/R_H}$$

$$R_H = -\left[2e\Gamma_m k_1 \frac{d\theta_H}{d\phi}\right]^{-1}$$

In the case that both R_∞ and R_p are positive, the impedance plot will result in two semicircles in the first quadrant,[27] as shown in Figure 7b. This is in agreement with the impedance plots observed experimentally at moderate overpotential (Figure 2a and b) (where one may safely assume $R_H \to \infty$). Now for potentials for which the polarization slope is negative, the impedance must enter the second quadrant. For the circuit of Figure 7a, this can occur in two ways (see Figure 7b):

(i) If $R_\infty/R_H > (k_1 + k_{ch})/k_2 n_s$, R_p becomes negative. However, R_∞ and C_p remain positive so that the impedance will not cross into the third quadrant, which is a necessary condition for having a Hopf bifurcation in the presence of an additional series resistor.[16] This is precisely equivalent to our earlier result that competetive adsorption can account for the negative slope but not for the oscillations. The impedance plot will have the form of Figure 7c.

(ii) If R_∞ is negative and smaller in absolute value than R_H (this latter condition is exactly the condition $\Delta_{T=0} > 0$ evaluated in the Appendix), both R_p and C_p will be negative as well and the impedance plot will enter the third quadrant for the lowest frequencies (because of the negative C_p). The impedance plot will have the form of Figure 7d. This coupling between a negative R_∞ and other elements (C_p and R_p, in this example) is well-known and also occurs in the Randles circuit[28] and other models of electrochemical impedance.[29] It is clear that only in this case can we anticipate the possibility of a Hopf bifurcation.

The impedance of this model still differs from the experimental impedance on two major points. First, at the highest frequencies, the impedance is always positive. It is reasonable to attribute this to a finite reaction rate of the hydride-layer formation. This is supported by a simulation of the electrical impedance including this effect, which results in an impedance plot shown as the solid line in Figure 8, in the negative slope region. This plot clearly shows that a finite rate of the hydride-layer formation does not invalidate the possibility of a Hopf bifurcation. A second, more serious deficiency of the present model is its inability to explain the inductive behavior observed outside the negative slope region and, related to this, to enter

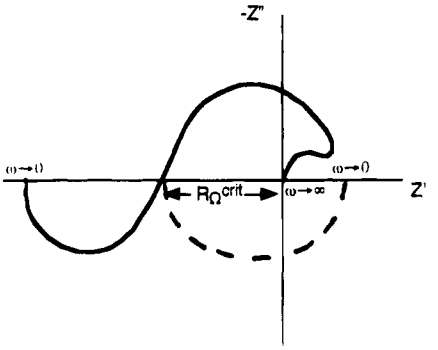

Figure 8. Complex impedance plane plot on the negative polarization slope region incorporating a finite rate of hydride-layer formation. The dashed line is the experimentally observed impedance as taken from Figure 2e. Both plots exhibit a Hopf bifurcation in the presence of an external resistor for the critical value R_Ω^{crit}. However, the dashed plot is likely to give oscillations under galvanostatic control, whereas the solid plot is not (see text).

the fourth quadrant from the third quadrant, as illustrated by the dashed plot in Figure 8. The latter is a necessary condition for having galvanostatic potential oscillations.[15,16] In fact, the transition from plot d to e in Figure 2 must be accompanied by a Hopf bifurcation in the galvanostat mode.[16,25] Plots c and d of Figure 2 indicate that the inductive behavior at the lowest frequencies is closely related (i.e., possesses a very similar time constant) to the capacitative behavior at slightly higher frequencies since the transition from one to the other occurs within less than a decade of the frequency and there is no clustering of points on the real impedance axis (as has been observed in other systems exhibiting inductive behavior[30]). The inductive loop (and, hence, the galvanostatic potential oscillations) persists for the other pH values we studied (0.3, 1.2, 2.5) and is also observed at the p-type material under illumination but is absent in a solution which does not contain H_2O_2, i.e., in the proton reduction (which exhibits two capacitative semicircles as its most essential feature).

When preparing the revised version of this paper, the recent paper by Pohlmann *et al.*[23] came to our notice, which presents a mathematical model for the current oscillations during H_2O_2 reduction on $CuInSe_2$. These authors also invoke the role of the hydride layer in causing the negative slope (in addition to hydroxide formation due to oxygen adsorption), but in their model, there is no necessity for a band-bending anomaly because it is assumed that the electron transfer occurs directly to a H_2O_2 molecule in the Helmholtz layer and not via a surface

intermediate. The necessary delay causing the time dependence of the interfacial H_2O_2 concentration is accounted for by diffusion from the bulk to the surface. Both effects do not apply to the H_2O_2 reduction on GaAs. First, there is ample evidence that a surface intermediate is involved in this reaction, and second, mass transport (disk rotation rate) does not have any influence on the faradaic current. Apart from that, as we already remarked above, there is some evidence for a band-bending anomaly in the H_2O_2 reduction on $CuInSe_2$ as well, from the electrolyte electroreflectance (EER) data presented by Cattarin *et al.*[6] Futhermore, it is not difficult to show that the model by Pohlmann *et al.* does also not support potential oscillations under galvanostatic conditions, whereas these are observed experimentally.

Conclusion

In this paper, we studied the current oscillations in the H_2O_2 reduction at n-type GaAs and attempted a mechanistic interpretation on the basis of a simple and tentative model which combines the model for H_2O_2 reduction at GaAs suggested by Minks *et al.*[13] with the (concurrent) H^+ reduction, which was treated following a suggestion made by Gerischer *et al.*[19] As our most important result, we have been able to establish that the current oscillations under fixed cell potential operation are due to a negative slope in the current−voltage curve, which must be caused by an increase in band bending with an increasingly negative potential (i.e., $d\phi_{sc}/d\phi < 0$), in conjunction with the ohmic resistance of the electrolyte solution.

The impedance measurements have confirmed that the H_2O_2 reduction at GaAs very likely proceeds via a surface intermediate and that in the potential region of the oscillations indeed follow $d\phi_{sc}/d\phi < 0$. The negative slope is attributed to the hydride intermediate in the H^+ reduction, which changes the charge distribution such as to increase the depletion layer band bending. The experimental evidence for this latter assumption is, however, still somewhat scant and deserves further investigation. The simple model as yet fails to explain the inductive loop observed in the impedance plots at moderate overpotential, as well as the potential oscillations under galvanostatic control.

Acknowledgment. We wish to thank Prof. John Kelly for his continuous interest in this work and for a critical reading of the manuscript.

Appendix

In this appendix, we concisely summarize the linear stability analysis of eq 21, leading to the conclusions of that section. Linearizing eq 21 about the steady state results in a set of homogeneous linear differential equations, the Jacobian matrix of which reads

$$\mathbf{J} = \begin{pmatrix} \epsilon^{-1}\dfrac{\partial F}{\partial \phi} & \epsilon^{-1}\dfrac{\partial F}{\partial \theta_1} \\ \dfrac{\partial G}{\partial \phi} & \dfrac{\partial G}{\partial \theta_1} \end{pmatrix}$$

where

$$\frac{\partial F}{\partial \phi} = -\frac{1}{R} + \frac{\partial \nu_2}{\partial \phi} \qquad \frac{\partial F}{\partial \theta_1} = \frac{\partial \nu_2}{\partial \theta_1} \qquad \frac{\partial G}{\partial \phi} = \frac{\partial \nu_1}{\partial \phi} - \frac{\partial \nu_2}{\partial \phi}$$

$$\frac{\partial G}{\partial \theta_1} = \frac{\partial \nu_1}{\partial \theta_1} - \frac{\partial \nu_2}{\partial \theta_1}$$

and

$$\frac{\partial \nu_1}{\partial \phi} = -k_1 \frac{\partial \theta_H}{\partial \phi} > 0 \qquad \frac{\partial \nu_1}{\partial \theta_1} = -k_1\left(1 + \frac{\partial \theta_H}{\partial \theta_1}\right) - k_{ch} < 0$$

$$\frac{\partial \nu_2}{\partial \phi} = \frac{\partial \nu_2}{\partial \phi_{sc}}\frac{d\phi_{sc}}{d\phi} = -\frac{e}{kT}k_2 n_s \theta_1 \frac{d\phi_{sc}}{d\phi} \qquad \frac{\partial \nu_2}{\partial \theta_1} = k_2 n_s > 0$$

(the signs are derived drom eqs 5, 6, and 19) where the partial derivatives are evaluated in the steady state. The eigenvalues $\{\lambda\}$ of the Jacobian are calculated from

$$\lambda^2 + T\lambda + \Delta = 0$$

with

$$T = -\epsilon^{-1}\frac{\partial F}{\partial \phi} - \frac{\partial G}{\partial \theta_1} \qquad \Delta = \epsilon^{-1}\left(\frac{\partial F}{\partial \phi}\frac{\partial G}{\partial \theta_1} - \frac{\partial F}{\partial \theta_1}\frac{\partial G}{\partial \phi}\right)$$

For a Hopf bifurcation, the condition $T = 0$ with $\Delta > 0$ has to be satisfied. $T = 0$ gives

$$\frac{\partial \nu_2}{\partial \phi} = \frac{1}{R} + \epsilon\left(\frac{\partial \nu_2}{\partial \theta_1} - \frac{\partial \nu_1}{\partial \theta_1}\right) > 0$$

which means that (i) $d\phi_{sc}/d\phi$ should be negative and (ii) there should a sufficiently large ohmic series resistance to let $1/R$ be small (ϵ should also not be very much larger than 1). The $\Delta > 0$ condition gives

$$\Delta_{T=0} = \epsilon^{-1}\left(-\epsilon\left(\frac{\partial \nu_1}{\partial \theta_1} - \frac{\partial \nu_2}{\partial \theta_1}\right)^2 + \left(\frac{\partial \nu_2}{\partial \phi} - \frac{\partial \nu_1}{\partial \phi}\right)\left(\frac{\partial \nu_2}{\partial \theta_1}\right)\right) > 0$$

This condition is satisfied in the (very) realistic limit of small ϵ, provided that $\partial\nu_2/\partial\phi > \partial\nu_1/\partial\phi$. This last condition is satisfied almost automatically if γ_H is sufficiently negative. This can be seen as follows. The term $\partial\nu_2/\partial\phi$ equals $-(e/kT)\nu_2(d\phi_{sc}/d\phi)$, and the term $\partial\nu_1/\partial\phi$ equals $(e/kT)k_1\theta_H(1 - \theta_H) \approx (e/kT)\nu_1\theta_H$ (where eq 25 has been used), and since in the steady state $\nu_1 = \nu_2$, it follows that the inequality $d\phi_{sc}/d\phi < -\theta_H$ must be satisfied. This condition can be satisfied with the reasonable values of γ_H considered in the main text. Note that the limit of small ϵ corresponds to so-called relaxation oscillations, i.e., highly nonlinear waveforms with fast transitions.

The case of the electrochemical cell under galvanostatic control corresponds to the limit $V \to \infty$ and $R \to \infty$ so that V/R = finite = J_{appl}. So the conditions for a Hopf become

$$\frac{\partial \nu_2}{\partial \phi} = \epsilon\left(\frac{\partial \nu_2}{\partial \theta_1} - \frac{\partial \nu_1}{\partial \theta_1}\right) > 0$$

and

$$\Delta_{T=0} = \epsilon^{-1}\left(\epsilon\left(\frac{\partial \nu_1}{\partial \theta_1}\right)\left(\frac{\partial \nu_2}{\partial \theta_1} - \frac{\partial \nu_1}{\partial \theta_1}\right) - \left(\frac{\partial \nu_1}{\partial \phi}\right)\left(\frac{\partial \nu_2}{\partial \theta_1}\right)\right) > 0$$

This last condition can never be satisfied, making the occurrence of a bifurcation to oscillations impossible in the galvanostatic mode.

References and Notes

(1) Lingane, J. J.; Lingane, P. J. *J. Electroanal. Chem.* **1963**, *5*, 411.
(2) Tributsch, H. *Ber. Bunsenges. Phys. Chem.* **1975**, *79*, 570, 580.
(3) Honda, M.; Kodera, T.; Kita, H. *Electrochim. Acta* **1986**, *31*, 377.
(4) Cattarin, S.; Tributsch, H. *J. Electrochem. Soc.* **1990**, *137*, 3475.
(5) Fetner, N.; Hudson, J. L. *J. Phys. Chem.* **1990**, *94*, 6506.
(6) Cattarin, S.; Tributsch, H.; Stimming, U. *J. Electrochem. Soc.* **1992**, *139*, 1320. Cattarin, S.; Tributsch, H. *J. Electrochem. Soc.* **1992**, *139*, 1328.
(7) Strbac, S.; Adzic, R. K. *J. Electroanal. Chem.* **1992**, *337*, 355.

(8) Koper, M. T. M.; Meulenkamp, E. A.; Vanmaekelbergh, D. *J. Phys. Chem.* **1993**, *97*, 7341.
(9) van Venrooij, T. G. J.; Koper, M. T. M. *Electrochim. Acta*, in press.
(10) Winkelmann, D. *Z. Elektrochem.* **1956**, *60*, 731.
(11) Memming, R. *J. Electrochem. Soc.* **1969**, *116*, 785.
(12) Minks, B. P.; Oskam, G.; Vanmaekelbergh, D.; Kelly, J. J. *J. Electroanal. Chem.* **1989**, *273*, 119.
(13) Minks, B. P.; Vanmaekelbergh, D.; Kelly, J. J. *J. Electroanal. Chem.* **1989**, *273*, 133.
(14) (a) Chizmadzev, Yu. A. *Dokl. Akad. Nauk USSR* **1960**, *133*, 745. (b) Degn, H. *Trans. Faraday Soc.* **1968**, *64*, 1348. (c) de Levie, R. *J. Electroanal. Chem.* **1970**, *25*, 257. (d) Koper, M. T. M. *Electrochim. Acta* **1992**, *37*, 1771.
(15) Epelboin, I.; Gabrielli, C.; Keddam, M. In *Comprehensive Treatise of Electrochemistry*; Bockris, J. O'M,; Conway, B. E.; Yeager, E.; White, R. E. Eds.; Plenum: New York, 1984; Vol. 4, p 151.
(16) Koper, M. T. M. Thesis, Universiteit Utrecht, 1994.
(17) Gray, P.; Scott, S. K. *Chemical Instabilities: Non-linear Chemical Kinetics*; Clarendon: Oxford, 1990.
(18) Gerischer, H.; Mindt, W. *Surf. Sci.* **1966**, *4*, 440.
(19) Gerischer, H.; Müller, N.; Haas, O. *J. Electroanal. Chem.* **1981**, *119*, 41.
(20) Laflère, W. H.; Cardon, F.; Gomes, W. P. *Surf. Sci.* **1974**, *44*, 541.
(21) Vanmaekelbergh, D.; Cardon, F. *J. Phys. D. Appl. Phys.* **1986**, *19*, 643.
(22) Schultze, J. W.; Vetter, K. J. *Ber. Bunsenges. Phys. Chem.* **1972**, *76*, 920, 927.
(23) Pohlmann, L.; Neher, G.; Tributsch, H. *J. Phys. Chem.* **1994**, *98*, 11007.
(24) Badawy, W. A.; Pfuhl, G.; Plieth, W. J. *J. Electrochem. Soc.* **1990**, *137*, 531.
(25) Koper, M. T. M.; Sluyters, J. H. *J. Electroanal. Chem.* **1994**, *371*, 149.
(26) Morrison, S. R. *Electrochemistry at Semiconductor and Oxidized Metal Electrodes*; Plenum: New York, 1980.
(27) Armstrong, R. D.; Henderson, M. *J. Electroanal. Chem.* **1972**, *39*, 81.
(28) (a) Sluyters-Rehbach, M.; Timmer, B.; Sluyters, J. H. *Z. Phys. Chem.* **1967**, *52*, 1. (b) de Levie, R.; Pospisil, L. *J. Electroanal. Chem.* **1969**, *22*, 277.
(29) Moreira, H.; de Levie, R. *J. Electroanal. Chem.* **1971**, *29*, 353.
(30) Vanmaekelbergh, D.; Searson, P. C. *J. Electrochem. Soc.* **1994**, *141*, 697.

JP942771T